Model for water transport into powdered xanthan combining gel swelling and vapor diffusion

U. Goerke
School of Physical Sciences, University of Surrey, Guildford, Surrey GU2 5XH, United Kingdom

A. H. L. Chamberlain
School of Biological Sciences, University of Surrey, Guildford, Surrey GU2 5XH, United Kingdom

E. A. Crilly
School of Physical Sciences, School of Biological Sciences, University of Surrey, Guildford, Surrey GU2 5XH, United Kingdom

P. J. McDonald*
School of Physical Sciences, University of Surrey, Guildford, Surrey GU2 5XH, United Kingdom
(Received 22 November 1999)

Water ingress into xanthan powder compressed to various packing densities has been studied using nuclear magnetic resonance stray field imaging (STRAFI). A foot is observed ahead of the main water ingress front which is attributed to vapor transport around the particles. The main development of the reported work is an analytical model which describes the coupling of vapor transport through the pore space and liquid transport through the progressively swelling gel which gradually occludes the vapor path. Good agreement between theory and experiment is found over a wide range of packing densities with the model requiring only one adjustable parameter, the water diffusivity in the gel measured in a constant polymer mass reference frame. It is suggested that the results are of considerable relevance to situations where the polymer is produced at low concentration by bacteria such as in the rhizosphere and aerial bio films.

PACS number(s): 81.05.Rm, 66.30.Ny, 76.60.Pc, 82.70.Gg

I. INTRODUCTION

Xanthan is one of a series of microbial polysaccharides which are well known for their ability to strongly interact with, and bind, large amounts of water. This property has lead to the suggestion that such biopolymers are produced by microorganisms to slow down water loss during desiccation in soils [1], in aerial bio films [2] and in marine environments subject to tidal exposure. It has further been suggested that the biopolymers prevent excessive water uptake when the bathing solution is very hypotonic, thus preventing damage due to water stress [3]. Xanthan is frequently used as a gelling and thickening agent, an emulsifier in food processing [4] and as a binder for pollutants in water. Considerable effort has been put into investigating structure-function relationships in order to better understand the interactions between water and ion transport properties and chemical structure of different xanthan types. Modern technology aims to tailor such properties for specific applications in the food and other industries.

Liquid transport in polymers in particular has been the subject of a number of investigations. A large variety of phenomena are observed ranging from Fickian diffusion where the mass uptake varies as the square root of time [5] to case II diffusion where mass uptake is linear with time [6]. The latter in particular results from the viscoelastic properties of the polymer. Most of these studies have concerned rubbery or glassy polymers presented as solid bulk material. There has also been some work looking at highly compressed pelleted material notably for drug release systems [7]. Other areas which have been studied include transport in gels and polymer dissolution [8]. However, there is considerably less work which attempts to measure water transport in loose agglomerations of polymer. This is exactly the form in which polysaccharides produced by bacteria are found in many natural desiccated environments. Here, the polymer is found at low concentration with considerable air space between agglomerates. The role of this air space in determining the water transport through the polymer is still under debate. The objective of this work is to measure water transport through aggregate polymer systems undergoing the dry-wet transition. We do this by using stray field magnetic resonance imaging to measure the time and space concentration dependence of water ingressing loosely packed, compared to tablets, xanthan powder beds. In addition, we introduce a model based on coupled liquid water and vapor diffusion to describe the data. It is based on our previous one which was introduced to describe the coupled transport in packed beds of zeolite powder [9]. It was subsequently found to be equally applicable to low level water diffusion in sandstones [10]. The key advance reported in this work is the inclusion of swelling which causes the vapor path to be occluded. Although the complexity of the mathematics is increased by swelling, we suggest that the generality of the model and the underlying physical considerations are of widespread importance.

There is considerable previous work on xanthan, particularly in relation to the food industry, but most of it is concerned with studies of viscosity and self-diffusion in aqueous gels and solutions. MRI is highly suited to the study of water dynamics in xanthan and indeed for liquids in polymers in

*Author to whom correspondence should be addressed.

general. Numerous previous examples of its satisfactory use for quantitative study can be cited including the seminal work of Blackband and Mansfield [11] and subsequent studies by, amongst others, Weisenberger and Koenig [12], Hyde *et al.* [13], and Narasimhan *et al.* [14]. This particular study follows on from our own previous work where we investigated the effect of chemical modification of the polysaccharide on water uptake [15].

II. SAMPLE PREPARATION AND EXPERIMENTAL METHODS

Keltrol F, a commercially available xanthan, was supplied as a lyophilised powder by Keltrol-Nutrasweet plc. (Epsom, UK). The xanthan powder was equilibrated in a desiccator above dry silica gel where it achieved a water fraction of 6 wt. %. Further drying was not possible without recourse to more extreme methods, which may radically alter the physical structure of the polymer. The dehydrated powder was loaded into the bore (2 mm inner diameter) of glass capillaries. It was compacted with two steel pins which were mounted in a press, one being attached to a screw. A known torque was applied on the screw to achieve reproducibility of compaction. The density of the sample was calculated from its mass, the length of the compacted powder column in the capillary and the cross section of the capillary. In the experiments, the top of the dry xanthan sample was exposed to deionized water. The time course of water ingress was profiled using stray field imaging (STRAFI).

Stray field imaging is a form of magnetic resonance imaging which exploits the very large magnetic field gradient found below superconducting magnets to achieve high spatial resolution at very short echo times [16,17]. The short echo times improve quantitation of the experiment since all the hydrogen nuclei in the sample are excited and observed. The standard multiple quadrature echo pulse sequence [16,17] was used, $90_x-\tau-[90_y-\tau-\text{echo}-\tau]_n-$ where $90_{x/y}$ signifies an excitation pulse of relative phase x or y and 2τ is the first echo time and n is the number of acquired echoes. The quadrature pulse sequence refocusses direct and stimulated echoes in phase and therefore obtains better signal to noise than the version using solely 90_x pulses. In the experiments reported here the gradient strength was 58 T/m, the pulse length was typically 6 μs corresponding to a slice width of 65 μm. The first echo time was typically 60 μs and n was 16. 30 slices were acquired at increments of 300 μm giving a profile length of 9 mm. The single profile acquisition time was 20 s and 64 averages were collected for signal averaging.

In order to still further improve the signal quantitation, uniformly equilibrated samples at various hydrations were also measured. For this purpose, xanthan samples were prepared by mixing the appropriate amounts of xanthan powder (Keltrol F) and water using a pestle and mortar. The samples were kept at 4 °C for a week to equilibrate. The xanthan samples were then quickly transferred into small test tubes and profiles acquired using exactly the same experimental setup and parameters as for the ingress experiments. A calibration curve (Fig. 1) was derived from the signal intensities and known hydrations of these samples to correct for residual signal attenuation due to T_2 and T_1 relaxation and diffusion, apparent even in STRAFI experiments.

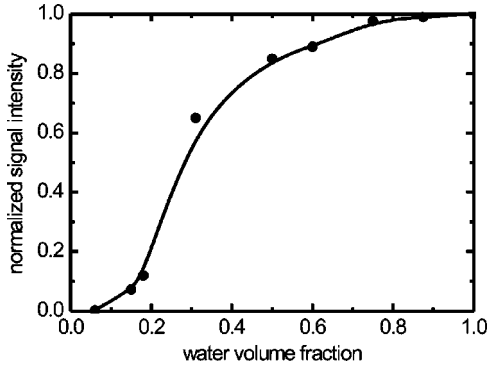

FIG. 1. Calibration curve for relaxation- and diffusion-weighted signal and corresponding water volume fraction c_w. The dots represent experimental data which were obtained from xanthan samples equilibrated at known water contents. The solid line is a cubic spline interpolation which was used for calibration.

Finally, the adsorption isotherm was measured for Keltrol F xanthan by equilibrating previously dehydrated material over a series of salt solutions of known water activity for 25 days [18] and measuring the mass uptake (Fig. 2).

III. MODEL DEVELOPMENT

A. Background

A model is suggested in which three regions are defined according to the principal operative diffusion mechanism (Fig. 3). Region 1 is a bed of loosely packed xanthan powder with initial void fraction κ_0. The water transport rate is primarily controlled by water vapor diffusion between the powder particles. As water is absorbed into the xanthan particles they swell, diminishing the void fraction. However, with void space still remaining, there is no overall expansion of the sample along the tube length. In region 2, it is assumed that the void space is completely filled with swollen xanthan and (liquid) water diffuses through a continuous gel matrix. The swelling causes macroscopic expansion of the gel with increasing water content. In region 3 the macromolecules disentangle and dissolve.

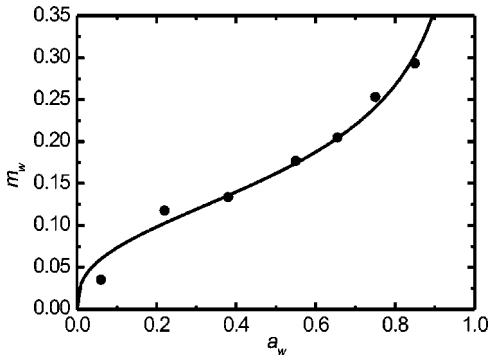

FIG. 2. Absorption isotherm of xanthan. The dots represent experimental data obtained from samples which were equilibrated over salt solutions of various water vapor activities a_w. m_w is the adsorbed water mass. The constants $A=0.162\ \text{g/cm}^3$ and $B=0.361$ were obtained by fitting (solid line) the Oswiin equation, Eq. (8), to the experimental data.

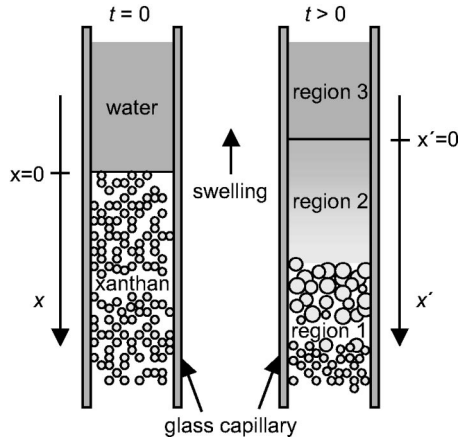

FIG. 3. Schematic of the compacted xanthan powder showing the three regions and two coordinate systems described in the text.

It is assumed that the diffusion obeys Fick's law in all three regions:

$$\frac{\partial c_w}{\partial t} = \frac{\partial}{\partial x}\left[D_{\mathrm{app}}(c_w)\frac{\partial c_w}{\partial x}\right], \tag{1}$$

where c_w is the volume fraction of water and D_{app} is an apparent diffusion coefficient referenced to the laboratory space and time coordinates x and t, respectively. Fickian diffusion implies that other processes, such as the condensation of water vapor onto xanthan particles and the local expansion of the polymer due to water uptake occur on time scales which are fast compared to the water transport. Consequently, in region 1, swelling xanthan particles and water vapor are always in local equilibrium according to the adsorption isotherm. In all regions the swollen gel matrix is in local equilibrium with the liquid water concentration. This results in an apparent diffusion coefficient D_{app}, which is, in general, a function of the water concentration c_w only.

For semi-infinite systems such as approximated by the current experimental setup, the Boltzmann transformation $\eta = x/(2\sqrt{t})$ can be applied to Eq. (1) to yield

$$0 = 2\eta\frac{dc_w}{d\eta} + \frac{d}{d\eta}\left[D_{\mathrm{app}}(c_w)\frac{dc_w}{d\eta}\right]. \tag{2}$$

The solution $c_w(\eta)$ of this differential equation of a single variable η is referred to as a master curve.

Given experimental master curves, it is possible to calculate $D_{\mathrm{app}}(c_w)$ using algorithms set out in the literature [11,19]. However, the calculation is notoriously sensitive to noise in the data. Moreover, this procedure does not provide insight into the diffusion mechanism. We prefer in this work to derive an analytical expression for $D_{\mathrm{app}}(c_w)$ for each of the three regions and from this to evaluate the master curve for comparison with data.

Equation (2) cannot be solved analytically for an arbitrary $D_{\mathrm{app}}(c_w)$. It is therefore solved numerically using standard forward differences and single step iteration methods

$$0 = \frac{c_i - c_{i-1}}{\eta_i - \eta_{i-1}}\left(2\eta_i + \frac{2D_i - D_{i-1}}{\eta_i - \eta_{i-1}}\right) - \frac{c_{i-1} - c_{i-2}}{(\eta_i - \eta_{i-1})(\eta_{i-1} - \eta_{i-2})}D_i. \tag{3}$$

Since the base of the sample is fixed within the capillary, swelling forces the polymer gel and solution in regions 2 and 3 to move upwards. To simplify the calculations, two space coordinate axes are used. The first, unprimed, coordinate x refers to the laboratory and maps onto the unprimed variable η. The origin is at the initial water/xanthan interface. The second, primed, coordinate system is fixed with respect to equal masses of polymer. The origin of this system is located at the dissolution interface between regions 2 and 3. The interface between regions 1 and 2 occurs at $\eta = \eta_{\kappa_0}$ where $c_w = \kappa_0$ and the interface between regions 2 and 3 at $\eta = -\eta_0'$ where $c_w = c_0$, the concentration required for dissolution. The solution of Eq. (2) can be found by various techniques. A convenient method is to set the value $c = c_0$ at $\eta = 0$ and, starting from an estimate of $dc/d\eta$, iteratively vary the gradient until the solution for which is $c \to 0$ as $\eta \to \infty$ is found. The solution is then transformed according to $\eta \to \eta - \eta_0'$. The local swelling of the polymer is according to $\delta\eta' = \delta\eta(c_P + \kappa_0)^{-1} = \delta\eta(1 - c_w + \kappa_0)^{-1}$, where c_P is the polymer concentration. The overall expansion of the gel region is proportional to the volume of water taken up by the polymer over and above the void space, assuming that no conformational change of the xanthan molecules occurs during expansion. The uptake is proportional to $\sqrt{t}$. It is given by $\int_{-\eta_0'}^{\eta_{\kappa_0}} (c_w - \kappa_0)(1 - \kappa_0)^{-1} d\eta$.

B. Region 1

Initially in region 1 vapor diffusion alone controls ingress dynamics. However, as vapor condenses on the xanthan particles and the particles swell, vapor diffusion is increasingly replaced by liquid water diffusion through the developing gel matrix. The mass transfer from vapor to water and local swelling of the particles is considered in a pair of coupled modified Fickian diffusion equations for both vapor and water as follows [20] :

$$\kappa(t)\frac{\partial m_v}{\partial t} = \frac{\partial}{\partial x}\left[\kappa(t) D_v \frac{\partial m_v}{\partial x}\right] - \frac{\partial S}{\partial t}, \tag{4}$$

$$[1 - \kappa(t)]\frac{\partial m_w}{\partial t} = \frac{\partial}{\partial x}\left[[1 - \kappa(t)] D_w \frac{\partial m_w}{\partial x}\right] + \frac{\partial S}{\partial t}, \tag{5}$$

where m_w and m_v are, respectively, the mass of liquid water per unit volume of polymer and the mass of vapor per unit volume of free void space. The void fraction at time t is denoted $\kappa(t)$ and D_v and D_w are, respectively, the vapor diffusion coefficient and water diffusion coefficient in the gel; the last being defined more carefully in the next section. The rate of water adsorption from the vapor phase onto the particles is $\partial S/\partial t$. The coupled equations, Eqs. (4) and (5), are replaced by a single equation with an apparent diffusion coefficient D_{app}. Since $\kappa m_v \ll (1 - \kappa) m_w$ for all κ of interest, it follows that, by adding Eqs. (4) and (5)

$$\frac{\partial m_w}{\partial t} \approx \frac{\partial}{\partial x}\left[D_{\text{app}} \frac{\partial m_w}{\partial x} \right] \tag{6}$$

with

$$D_{\text{app}} = \frac{\kappa(t)}{1-\kappa(t)} D_v \frac{\partial m_v}{\partial m_w} + D_w, \quad c_w \leqslant \kappa. \tag{7}$$

The vapor and liquid water are in local equilibrium. It is assumed that the adsorption isotherm for Keltrol F xanthan can be fitted to the Oswiin equation [21]:

$$m_w = A\left(\frac{a_w}{1-a_w} \right)^B, \tag{8}$$

where A and B are constants characteristic of the polysaccharide and a_w is the water vapor activity. The activity is related to m_v by $m_v = a_w m_v^0$ where m_v^0 is the mass of vapor per unit volume of void above liquid water. Bearing in mind that $m_w(c_w) = c_w \rho_w / (1-\kappa_0)$, where ρ_w is the density of water, it follows that

$$D_{\text{app}}(c_w) = \frac{\kappa_0 - c_w}{1-(\kappa_0 - c_w)} D_v \frac{m_v^0}{B m_w} \frac{(m_w/A)^{1/B}}{[(m_w/A)^{1/B}+1]^2} + D_w \tag{9}$$

an expression which is valid for $c_w \leqslant \kappa_0$. The water vapor density m_v^0 is calculated from the water vapor pressure at 20 °C, 234 Pa [22]. Given a value of the atmospheric pressure of 10133 Pa, the molar mass of water, 18.01 g/mol and the molar volume of gas, 24 L/mol, then the density of water vapor, m_v^0, is 1.73×10^{-5} g/cm^3.

Vapor diffusion takes place in the free pore space between the xanthan particles. Similar porous systems are described as percolation networks which often show a fractal structure [23]. However, the geometry of the pore space is unknown especially since the particles can be deformed in the compressed powder. Furthermore, water is adsorbed on the particles and therefore the geometry changes with water concentration. In this paper a phenomenological approach to describe the pore space is adopted. The vapor diffusion coefficient is reduced by a factor equal to the pore space tortuosity τ which describes the decrease of the mean square displacement due to obstacles in the diffusion pathway. To simplify the analysis, a constant tortuosity with respect to water concentration is assumed so that

$$D_v = \frac{D_v^{\text{free}}}{\tau}. \tag{10}$$

The water vapor diffusion coefficient in air is known from literature to be $D_v^{\text{self}} = 2.5 \times 10^{-5}$ m^2/s [24]. For the simulation a tortuosity of $\tau = 3$, which is typical for many porous systems [25], is used. Hence, the effective vapor diffusion coefficient is $D_v = 8 \times 10^{-6}$ m^2/s.

A master curve for region 1, based on the adsorption isotherm parameters for Keltrol F xanthan to be presented in the next section and at a compaction typical of our experiments, $\kappa_0 = 0.3$ and $D_w = 10^{-10}$ m^2/s, is shown in Fig. 4(a). The water concentration at $\eta = -\eta_0'$ is kept constant, $c_w = c_0$. This master curve is compared to the master curve which results from a constant value $D_{\text{app}} = 10^{-10}$ m^2/s. The comparison makes clear how vapor diffusion in the pore space leads to the formation of a foot ahead of the main ingress front.

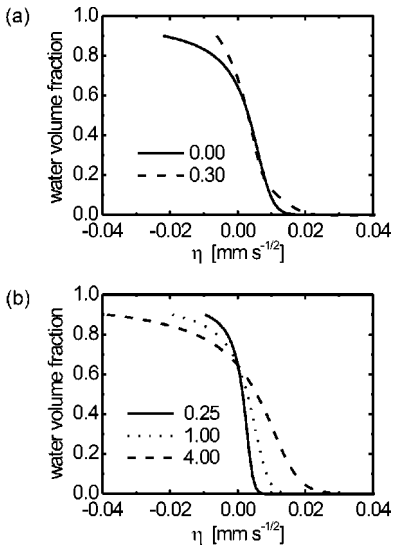

FIG. 4. (a) Two calculated master curves for two different initial free pore space fractions $\kappa_0 = 0.00$ for a completely compacted sample (solid line) and $\kappa_0 = 0.30$ (dashed line). The ''foot'' ahead of the main water front for the larger value of κ_0 is observed. The shift of the left most end of the curves at $\eta = \eta_0'$ and $c_w = c_0 = 0.9$ is caused by macroscopic expansion of the xanthan sample corresponding to the water/xanthan interface moving upwards due to swelling. The more compacted sample $\kappa_0 = 0.00$ shows a more pronounced shift, hence a greater expansion. (b) Calculated master curves for different liquid water diffusion coefficients D_w in xanthan for samples with no free pore space $\kappa_0 = 0.00$. The numbers in the figure represent $D_w/(10^{-10}$ m^2/s). The curve with the highest diffusion coefficient shows the greatest extension to the right and to the left indicating faster water transport into the sample as well as the largest expansion of the polymer, respectively. The curves intersect at $\eta = 0.0$.

C. Region 2

In region 2, mass transport occurs as a result of water diffusion driven by the concentration gradient and swelling caused by the water uptake. The latter results in a flow of polymer and water relative to the laboratory-fixed coordinate system in the opposite direction to the ingressing water. In the proposed model it is assumed that the swelling is faster than the ingress and therefore that the polymer matrix is free of mechanical stress. Both water diffusion and expansion of the polymer gel need to be considered in the apparent diffusion coefficient D_{app}. Assuming that there is no volume change on mixing, that is, the individual densities for water and xanthan are constant, total volume is conserved $c_P + c_w = 1$ and therefore the swelling of the xanthan is directly related to the water concentration. In the laboratory fixed reference frame the apparent diffusion coefficient is then given by [19]

$$D_{\text{app}} = D_w (1 - c_w + \kappa_0)^{-2}, \tag{11}$$

where D_w is the diffusion coefficient of water in the continuous polymer gel measured in the primed polymer-mass fixed

coordinate system. That is, it is the diffusion coefficient relative to equal amounts of polymer. The factor in brackets corrects for swelling of the polymer to give a diffusion coefficient in the laboratory frame.

In general, the water diffusion coefficient D_w is a function of the water concentration c_w. A general model for the swelling of polymers without void space was suggested by Gao and Mackley [26]. However, for polysaccharides in particular there is little information on the concentration dependence of D_w available. Without *a priori* information, we choose to keep D_w constant. In practice this choice leads to a diffusion coefficient in the laboratory frame D_{app} which increases markedly with water concentration. Such an increase is not unlike other arbitrary forms of transport diffusion coefficient for liquids in polymers, such as exponential increases, to be found in the literature [14].

Master curves for region 2 for different values of water diffusion coefficients D_w, are shown in Fig. 4(b) for the case of a fully compacted sample (no free pore volume: $\kappa_0=0$, no region 1) and $c_0=0.9$. These curves make clear the existence of an effective surface at $x=0$ (transformed to $\eta=0$) from which the diffusion appears to eminate. The location $\eta'=0$ occurs at the extreme left hand end of the curves where $c_0=0.9$. Clearly the sample swells more rapidly as D_w is increased.

D. Region 3

Dissolution, that is mass transport of polymer across the gel/solution interface between regions 2 and 3, is determined by the rate at which polymer chains disentangle and dissolve as well as the rate of water diffusion into the bulk material. In the unstirred solution the dissolution rate of the polymer at the interface is determined by the diffusion flux of water across the boundary. Since xanthan is a slowly dissolving high-molecular weight polymer, an equilibrium water concentration at the interface is not reached until after an induction period with a time constant which is a function of the disentanglement time, the mutual diffusion coefficient in the solution and the water diffusion coefficient in xanthan. The transient process $[c_0=c_0(t)]$ is beyond the scope of this paper. Further results will be discussed assuming equilibrium at the interface. The loss of polymer causes the interface between regions 2 and 3 at $\eta'=0$ to shift by a small distance $\Delta\eta'$. Since xanthan dissolves only at a very high water fraction, in excess of 90% [15], this shift is always very much smaller than the shift due to swelling and can be safely neglected.

IV. RESULTS AND DISCUSSION

Water ingress into Keltrol F xanthan experiments were performed on five samples at different levels of compaction. The void fraction was calculated from the known mass of the xanthan and its volume under the assumption that the most compacted sample contained no free space between the particles. The void fraction for the five samples ranged from 0.00 to 0.65. Figure 5(a) shows a typical set of ingress profiles from a sample with $\kappa_0=0.4$. The profiles shown were recorded at intervals of about 21 min. The profiles were constructed from a summation of echoes 13 to 16. This choice offered the best contrast between the polymer and the water

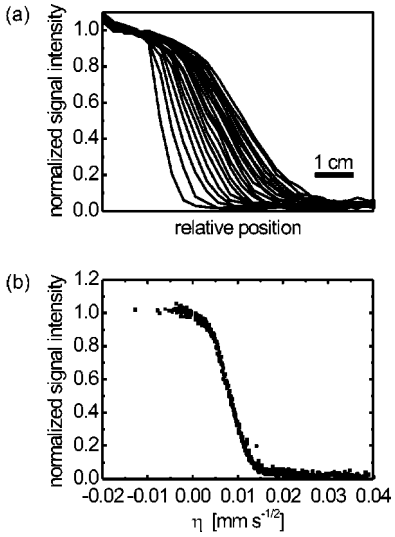

FIG. 5. (a) A typical set of experimental water ingress profiles ($\kappa_0=0.40$) as a function of time. The water reservoir is on the left and the dry xanthan powder on the right hand side. The curves were calculated from the sum of the last four echoes in trains of 16 echoes. The spatial resolution is 300 μm. The time interval from one profile to the next is about 21 min. The curves are normalized to the signal intensity of the water reservoir. These curves are relaxation and diffusion weighted. (b) Boltzmann-transform of the experimental data set in (a). Since the diffusion process is Fickian the profiles collapes onto a single curve.

signal. The signal intensities were normalized to that of the water reservoir in the first profile. In order to confirm Fickian diffusion dynamics and to accurately locate the initial interface between water and xanthan, the position of half-amplitude of the profile, x_f, was plotted against $\sqrt{t}$. The location $x=0$ is obtained by linear extrapolation of this plot to $t=0$. The experimental master curve was obtained by Boltzmann transformation $\eta=x/(2\sqrt{t})$ of the entire data set and is shown in Fig. 5(b).

In order to test the model presented in the previous section, it is necessary to evaluate $D_{\mathrm{app}}(c_w)$. In order to minimize the number of free parameters, as many as possible are obtained from other sources. Figure 2 shows the measured absorption isotherm for xanthan together with a fit according to the Oswiin equation. The fit parameters are $A=0.162$ g/cm^3 and $B=0.361$ for Keltrol F xanthan. The position $x=0$ and the void fraction κ_0 were derived as above and c_0 was set to 0.9 in accordance with previous MRI and chemical analysis measurements [15]. The vapor diffusion coefficient and tortuosity were fixed as discussed in the previous section. The only remaining free parameter is therefore D_w which was treated as a free fitting parameter. However, it was a requirement that D_w was a constant across all five samples.

Figure 6 shows best fit theoretical master curves compared to experimental data for five samples. The data points for samples with $\kappa_0>0$ are systematically shifted one to the next along the ordinate and the abscissa by 0.1 and 0.02 mm/s$^{1/2}$, respectively. The number above each curve represents the calculated free volume fraction κ_0 rounded to the closest multiple of 0.05. The theoretical curves have been weighted with T_2 and diffusion using the measured calibra-

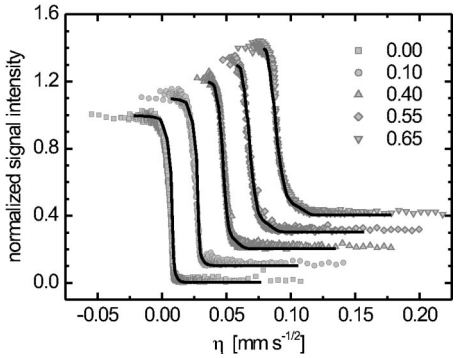

FIG. 6. Boltzmann transforms (symbols) of experimental water ingress profiles of five samples of different levels of compaction and corresponding computed master curves (solid lines) which were weighted according to the attenuation of signal intensity in the experiment. The values for the initial free pore space volume fraction, κ_0 (values given in the graph) are calculated on the assumption that the most compacted sample contains no free pore space $\kappa_0=0.00$. All the theoretical curves were calculated using $D_w=1.3\times10^{-10}$ m^2/s. This value was chosen to give best overall coincidence with the five experimental curves.

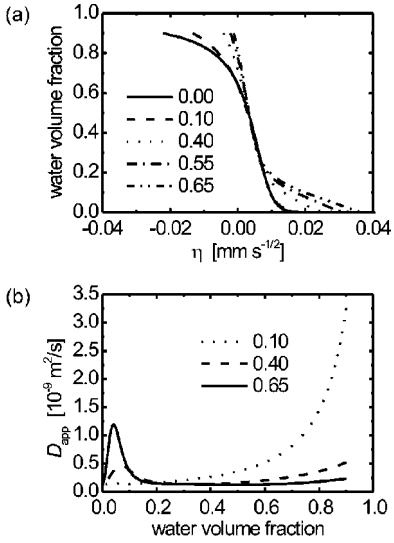

FIG. 7. (a) Calculated (no relaxation- and diffusion-weighting) master curves for the data sets in Fig. 6. The values in the graph represent the initial free pore space volume fraction κ_0. The curves show clearly the ''foot'' ahead of the water ingress front resulting from water vapor diffusion at high values of κ_0. For small values of κ_0 the expansion of the polymer is more pronounced, resulting in a greater shift of the curve to the left. (b) The apparent diffusion coefficient $D_{\rm app}$ versus the water volume fraction c_w as it results from the computation of the master curves in (a). The corresponding values of the initial free pore space volume fraction κ_0 are given in the graph. The higher the κ_0, the larger the local maximum at $c_w\approx0.05$ which is caused by vapor diffusion and leads to the ''foot'' in the master curves. The curvature at higher water volume fraction is a result of the superposition of the motion of the expanding polymer and the liquid water diffusion coefficient in the polymer-mass fixed coordinate system.

tion curve, shown in Fig. 1, deduced from uniformly equilibrated samples in order that they can be compared directly to experimental data. The best fits were obtained using $D_w=1.3\times10^{-10}$ m^2/s. Considering that all parameters apart from the compaction level were kept constant for all five samples, the agreement between theory and experiment is very good. At higher values of the free pore space fraction κ_0 the extension of the master curve foot due to vapor diffusion at low water concentration becomes apparent. The scattering of the experimental data points in this region is probably due to inhomogeneous compaction of the powder. More careful inspection of the data suggests that the model overestimates the diffusion at low values of κ_0 and underestimates it at higher values. In part, we suggest that this is because neither D_v/τ nor D_w are necessarily constants. Undoubtedly, better fits can be obtained by introducing concentration dependence of these parameters. It is also probable that the most compacted sample retains a finite pore volume, so introducing a systematic error into the calculated κ_0 values. We have been unable to find a true measure of xanthan density in the literature and our own attempts to measure it by carefully dissolving small quantities of xanthan in water have not been sufficiently accurate to answer the question.

Figure 7(a) shows the same theoretical master curves but without correction for signal attenuation. These curves make more obvious the differences at high water fraction. The strong swelling of the xanthan gel reveals itself in the highly curved upper part of the master curve and its shift to negative values of η especially for small κ_0. The shape of the theoretical master curves is sensitive to the parameter c_0. In particular, the intersection with $\eta=0$ varies with c_0. However, the fits are not significantly improved by varying c_0 from the otherwise preferred value of 0.9.

Finally Fig. 7(b) shows $D_{\rm app}$ as a function of c_w for three values of κ_0. At water fractions above κ_0 the diffusion coefficient increases markedly for high packing densities, consistent with previous ideas in the literature. This occurs even though the diffusivity in a polymer-mass fixed reference frame is considered constant. The new feature coming forward in this work is the local maximum ocurring at $c_w\approx0.05$. This is entirely due to the influence of the vapor diffusion and is likely to be significant in situations where polymers naturally occur, such as in the rhizosphere. It is likely to be as important as variations in $D_{\rm app}$ which occur due to natural chemical modification and variability of the polysaccharides arising from strain to strain variation within the microbial community and as a result of changes in environmental and nutritional parameters [27,28].

V. CONCLUSIONS

Experiments have shown that free pore space in lightly compacted polysaccharide powder beds has a significant influence on water transport through the bed. A model has been introduced which couples vapor transport in the pore space with liquid transport through a swelling gel. Reasonable agreement between theory and experiment has been found for the model with only one adjustable parameter, the water diffusivity through the polymer gel in polymer mass fixed reference frame. Further experiments which attempt to couple the combined effects of packing density and chemical variability are in progress.

ACKNOWLEDGMENTS

We thank Dr. Tim Hart, School of Biological Sciences, University of Surrey, for help in generating the adsorption isotherm data. E.A.C. would like to thank the Daphne Jackson Memorial Fellowships Trust for financial support. This work is partially funded by the U.K. Engineering and Physical Sciences Research Council under Grant No. GR/M00268.

[1] C. Chenu, Geoderma **56**, 143 (1993).
[2] C. Grant, C. A. Hunter, B. Flannigan, and A. F. Bravery, Int. Biodeterioration **25**, 259 (1989).
[3] T. L. Kieft, E. Soroker, and M. K. Firestone, Soil Biol. Biochem. **19**, 119 (1987).
[4] B. Katzbauer, Polym. Degrad. Stab. **59**, 81 (1998).
[5] B. De'Neve and M. E. R. Shanahan, Polymer **34**, 5099 (1993).
[6] N. L. Thomas and A. H. Windle, Polymer **23**, 529 (1982).
[7] L. S. Cutts, S. Hibberd, J. Adler, M. C. Davies, and C. D. Melia, J. Controlled Release **42**, 155 (1996).
[8] J. S. Vrentas and C. M. Vrentas, J. Polym. Sci. **36**, 2607 (1998).
[9] P. D. M. Hughes, P. J. McDonald, M. R. Halse, B. Leone, and E. G. Smith, Phys. Rev. B **51**, 11 332 (1995).
[10] P. J. McDonald, T. Pritchard, and S. P. Robert, J. Colloid Interface Sci. **177**, 439 (1996).
[11] S. Blackband and P. Mansfield, J. Phys. C **19**, L49 (1986).
[12] L. A. Weisenberger and J. L. Koenig, Macromolecules **23**, 2445 (1990); **23**, 2454 (1990).
[13] T. M. Hyde, L. F. Gladden, M. R. Mackley, and P. Gao, J. Polym. Sci., Part A: Polym. Chem. **33**, 1795 (1995).
[14] B. Narasimhan, J. E. M. Snaar, R. W. Bowtell, S. Morgan, C. D. Melia, and N. A. Peppas, Macromolecules **32**, 704 (1999).
[15] T. D. Hart, A. H. L. Chamberlain, J. M. Lynch, B. Newling, and P. J. McDonald, Enzyme Microb. Technol. **24**, 339 (1999).
[16] A. A. Samoilenko, D. Y. Artemov, and L. A. Sibeldina, JETP Lett. **47**, 417 (1988).
[17] P. J. McDonald and B. Newling, Rep. Prog. Phys. **61**, 1441 (1998).
[18] P. W. Winston and D. H. Bates, Ecology **41**, 232 (1960).
[19] J. Crank, *The Mathematics of Diffusion* (Clarendon Press, Oxford, 1975).
[20] P. D. M. Hughes, P. J. McDonald, and E. G. Smith, J. Magn. Reson., Ser. A **121**, 147 (1996).
[21] A. Bassal, J. Vasseur, and A. Lebert, J. Food. Sci. **58**, 449 (1993).
[22] D. R. Lide, *Handbook of Chemistry and Physics*, 72nd ed. (CRC, Boca Raton, 1991).
[23] M. Sahimi, *Flow and Transport in Porous Media and Fractured Rock: From Classical Methods to Modern Approaches* (VCH, Weinheim, 1995).
[24] E. H. Kennard, *Kinetic Theory of Gases* (McGraw-Hill, New York, 1938).
[25] E. L. Cussler, *Diffusion — Mass Transfer in Fluid Systems* (Cambridge University Press, Cambridge, England, 1984).
[26] P. Gao and M. R. Mackley, Proc. R. Soc. London, Ser. A **444**, 267 (1994).
[27] A. Sanchez, M. E. Ramirez, L. G. Torres, and E. Galindo, World J. Microbiol. Biotechnol. **13**, 443 (1997).
[28] H. Umashankar, G. Annadurai, M. Chellapandian, and M. R. V. Krishnan, Bioprocess. Eng. **14**, 307 (1996).